17th Brazilian Congress of Thermal Sciences and Engineering
November 25th-28th, 2018, Águas de Lindóia, SP, Brazil

ENCIT-2018-0204
CFD SIMULATION OF A RANQUE-HILSCH VORTEX TUBE WITH 3 INLETS AND EXPERIMENTAL VALIDATION

David Oliveira Almeida
Paulo Alexandre Costa Rocha
Maria Eugênia Vieira da Silva
Hugo Alberto López Clemente
Federal University of Ceará (UFC) , Av. Da Universidade, 2853 – Benfica, Fortaleza – CE, 60020-181, Brazil
david.o.almeida@hotmail.com
paulo.rocha@ufc.br
eugenia@ufc.br
hlopezc-10@outlook.com

Abstract. *A Ranque-Hilsch vortex tube is an equipment with no moving parts that uses Ranque effect to generate two streams from pressurized gas: a colder one and a hotter one. Due to its relevance in alternative refrigeration methods, the vortex tube has been studied for analysis purposes employing experimental and computational methods. The present work aims to analyze the Ranque effect using CFD methods in vortex tubes with 3 inlets and a L/D ratio of 40. For this purpose, it was used ICEM® mesh generator using blocking technique to obtain hexahedral meshes for vortex tube. Thereafter theses meshes were used to run CFD simulations in FLUENT® utilizing ideal gas e k-e turbulence model for steady state analysis. Results of CFD simulations of vortex tube at 2 bar showed a good accordance with experimental data. However, same simulation at 3 and 4 bar haven't been as accurate as 2 bar tests, predicting thermal separation effect in a higher magnitude than expected.*

Keywords: *Vortex tube, CFD, FLUENT®*

1. INTRODUCTION

The Ranque-Hilsch vortex tube is a mechanical device created by Ranque (1993) and subsequently modified and enhanced by Hilsch (1947). A schematic drawing showing it is presented in Figure 1. It works receiving a pressurized gas into a vortex chamber which promotes a swirling flow inside of it. As long as the fluid flows inside the vortex tube, two streams are generated: one colder and other hotter than the inlet stream. That phenomenon is called Ranque-effect, temperature separation effect or energy separation and its cause has not yet been fully explained. In counter flow vortex tubes, cold and hot streams flows at opposite ends – cold and hot ends respectively. A control valve is installed at the hot end to restrain the hot stream and deviate it towards the cold end.

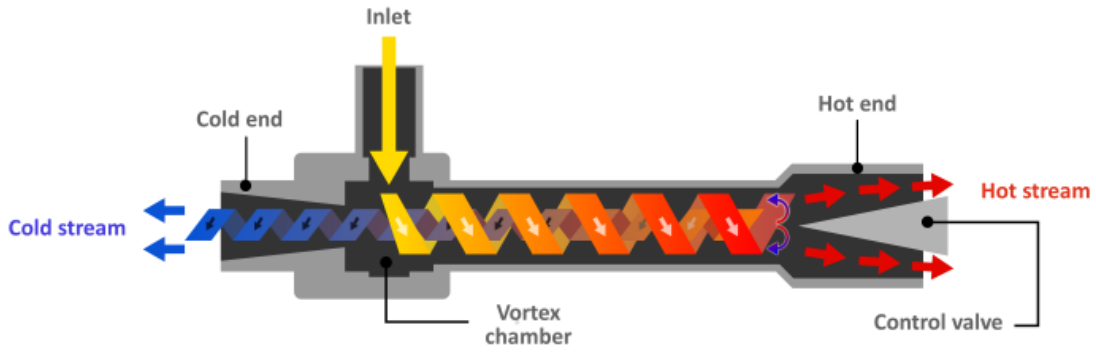

Figure 1. Schematic drawing of a vortex tube.
(Adapted from https://www.airtx.net/)

Since the vortex tube has no moving parts, it requires low or no maintenance and it has great life time. Also, it's a simple, light and compact device with low initial cost. Moreover, it represents itself as a good alternative refrigeration

device since no refrigerant gas is used to generate the cold stream, unlike vapor-compression refrigeration systems. Although its advantages, the vortex tube has an increased operational cost if compressed gas is not available. Another disadvantage is its low COP and low capacity for refrigeration use.

Some studies were performed using CFD techniques. Skye, et al., (2006) created a two dimensional axis-symmetric CFD model of a commercial vortex tube using k- ε and RNG k-ε turbulence models. Their model had some good accuracy in predicting the energy separation effect. They also concluded that the use of k-ε model leads to better results than RNG k- ε. However, that model was not capable to evaluate some geometry features of the vortex tube like inlet shape and vortex chamber geometry, because it was a two dimensional model with some intrinsic simplifications. Many others researchers followed Skye, et al., (2006) model methodology like Secchiaroli, *et al.*, (2009), Pouraria and Zangooee (2012), Kandil and Abdelghany (2015) and Thakare and Parekh (2015) contributing with other aspects not covered by the first one. Behera et al. (2005) performed vortex tube simulations modeling a tridimensional sector of the whole vortex tube geometry and applying symmetry boundary condition on start and end sector planes. They used RNG k-ε turbulence model and accomplished good qualitative results. Others works done by Behera *et al.*, (2008), Dutta, Sinhamahapatra and Bandyopadhyay (2011), Baghdad *et al.*, (2011) and Ouadha, Baghdad and Addad (2013) used the same model strategy. The model using tridimensional sector with symmetry boundary condition may lead to inaccuracies but it represents a good alternative if compared to two dimensional models. As a result of computational resources improvements over the years, complete tridimensional models were able to be employed by Secchiaroli *et al.*, (2009), Rafiee and Rahimi (2013), Rafiee and Sadeghiazad (2014), Manimaran (2017) and Rafiee and Sadeghiazad (2017).

This work aims to conduct an experimental and a numerical study using a full tridimensional model to evaluate the Ranque-Hilsch effect and vortex tube performance. As soon as these objectives are achieved, results from this work will establish a basis for future analysis in order to achieve vortex tube operational improvements.

2. METHODOLOGY

This section presents the methodology employed to carry out the experimental and numerical studies of the vortex tube. Experimental studies consist of laboratory tests of vortex tube with appropriate measuring instruments. Numerical studies were made using Computational Fluid Dynamics (CFD) techniques.

2.1 Experimental study

Experimental tests were conducted employing a vortex tube with characteristics described in Table 1. A schematic presentation of the setup utilized to carry out the tests of the vortex tube is shown in Figure 2. The measuring instruments employed in the experimental setup have their specification presented in Table 2. Several experiments were carried out using compressed air at 2, 3 and 4 bar.

Table 1. Vortex tube characteristics.

Length	460 mm
Diameter of the main tube	11.5 mm
Diameter of the cold end	8 mm
Number of inlet nozzles	3

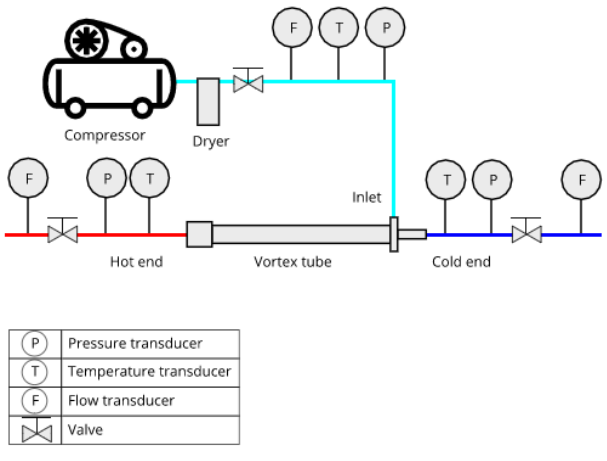

Figure 2. Experimental setup of the vortex tube tests.

Table 2. Measuring instruments specifications.

Item		Specifications
Temperature Transducer	Type	Thermocouple, type K
	Reference	Omega
	Range	-200 to 1250ºC
	Accuracy	±0.75%
Pressure Transducer	Type	Capacitive
	Reference	Omega PX309-100G5V
	Range	0 to 100 psi
	Accuracy	±0.25%
	Operating temperature	-20 to 85ºC
Flow Transducer	Type	Rotameter
	Reference	Dwyer RMC-107-SSV
	Range	120 to 1200 CFH
	Accuracy	±2%
	Operating pressure	0 a 100 psi

In all experiments, the following vortex tube operational parameters could be measured:

a) Cold mass fraction α: ratio of the cold mass stream $\dot{m}_c$ to inlet stream $\dot{m}_{in}$, given as:

$$\alpha = \frac{\dot{m}_c}{\dot{m}_{in}} \tag{1}$$

b) Cold end temperature difference ΔT_c: difference between the inlet gas temperature T_{in} and cold end gas temperature T_c, given as:

$$\Delta T_c = T_{in} - T_c \tag{2}$$

c) Hot end temperature difference ΔT_h: difference between the hot end gas temperature T_h and the inlet gas temperature T_{in}, given as:

$$\Delta T_h = T_h - T_{in} \tag{3}$$

d) Total temperature difference ΔT: difference between the hot end gas temperature T_h and the cold end gas temperature T_c, given as:

$$\Delta T = T_h - T_c \tag{4}$$

2.2 Numerical study

2.2.1 Governing equations

The flow inside a vortex tube using air is modeled as compressible flow problem. The conservation equations of a steady-state system involving the phenomena of flow and heat transfer in a compressible fluid solved by CFD techniques are shown below.

Mass conservation equation

The principle of mass conservation applied to a small volume element without source terms leads to:

$$\nabla \cdot \left(\rho \vec{v} \right) = 0 \tag{5}$$

where ρ and $\vec{v}$ are fluid density and its velocity field.

Momentum conservation equation

Conservation of momentum in an inertial reference frame is described by:

$$\nabla \cdot \left(\rho \vec{v} \vec{v} \right) = -\nabla p + \nabla \cdot \bar{\bar{\tau}} + \rho \vec{g} + \vec{F} \tag{6}$$

where p, $\bar{\bar{\tau}}$, $\vec{g}$ and $\vec{F}$ are, respectively, static pressure, stress tensor, gravity and external forces. The stress tensor $\bar{\bar{\tau}}$ is given by:

$$\bar{\bar{\tau}} = \mu \left[\left(\nabla \vec{v} + \nabla \vec{v}^{T} \right) - \frac{2}{3} \nabla \cdot \left(\vec{v} I \right) \right] \tag{7}$$

where μ is molecular viscosity and I is the unitary tensor.

Energy conservation equation

As a result of application of the first law of thermodynamics, the energy conservation equation is described by:

$$\nabla \cdot \left[\vec{v} \left(\rho E + p \right) \right] = \nabla \cdot \left(k_{t-eff} \nabla T + \bar{\bar{\tau}}_{eff} \cdot \vec{v} \right) \tag{8}$$

where k_{t-eff} is the effective thermal conductivity and $\bar{\bar{\tau}}_{eff}$ is the effective stress tensor. The total volumetric energy, *E*, is defined by:

$$E = h - \frac{p}{\rho} + \frac{v^2}{2} \tag{9}$$

where $h = \int_{T_{ref}}^{T} C_p dT$ and T_{ref} = 298.15 K.

Ideal gas equation

The ideal gas equation for compressible flows is given by:

$$\rho = \frac{p_{op} + p}{\frac{R}{M_w} T} \tag{10}$$

where *p* is the relative pressure, p_{op} is the operational pressure and M_w is the molecular weight.

Air properties equation

Air properties like viscosity, thermal conductivity and specific heat at constant pressure were determined by a polynomial of degree 3 with coefficients presented in **Erro! Fonte de referência não encontrada.**.

$$\phi(T) = a_0 + a_1 T + a_2 T^2 + a_3 T^3 \tag{11}$$

Table 3. Coefficients for the determination of air properties.

	a_0	a_1	a_2	a_3
$c_p\ (J\ kg^{-1}K^{-1})$	1015.9683	-0.12802	2.94104E-4	2.93413E-8
$\mu\ (kg\ m^{-1}s^{-1})$	-2.61819E-7	8.04006E-8	-7.04884E-11	3.50834E-14
$k_t\ (W\ m^{-1}K^{-1})$	-8.07779E-4	1.04110E-4	-5.11705E-8	1.56157E-11

Turbulence equations for standard k-ε model

The standard k- ε turbulence model was employed to evaluate transport of turbulent kinetic energy, *k*, and its rate of dissipation, ε:

$$\frac{\partial}{\partial x_i}\left(\bar{\rho}k\tilde{u}_i\right)=\frac{\partial}{\partial x_j}\left(\mu+\frac{\mu_t}{\sigma_k}\frac{\partial k}{\partial x_j}\right)+G_k+G_b-\bar{\rho}\varepsilon-Y_M+S_k \tag{12}$$

$$\frac{\partial}{\partial x_i}\left(\bar{\rho}\varepsilon\tilde{u}_i\right)=\frac{\partial}{\partial x_j}\left(\mu+\frac{\mu_t}{\sigma_\varepsilon}\frac{\partial \varepsilon}{\partial x_j}\right)+G_{1\varepsilon}\frac{\varepsilon}{k}\left(G_k+C_{3\varepsilon}G_b\right)-C_{2\varepsilon}\rho\frac{\varepsilon^2}{k}+S_\varepsilon \tag{13}$$

where $G_{1\varepsilon}$, $C_{2\varepsilon}$ and $C_{3\varepsilon}$ are constants; σ_k and σ_ε turbulent Prandtl numbers and S_k and S_ε are source terms. G_k, G_b and Y_M are calculated by:

$$G_k=-\overline{\rho u_i^{"}u_j^{"}}\frac{\partial \tilde{u}_j}{\partial x_i}=\mu_t S^2 \qquad S=\sqrt{2S_{ij}S_{ij}} \tag{14}$$

$$G_b=g_i\frac{\mu_t}{\bar{\rho}\,\mathrm{Pr}_t}\frac{\partial \bar{\rho}}{\partial x_i} \tag{15}$$

$$Y_M=2\bar{\rho}\varepsilon M_t^2 \qquad M_t=\sqrt{\frac{k}{a^2}} \tag{16}$$

where S_{ij} is fluid strain rate, g_i is the gravity component and Pr_t is the energy Prandtl number. The turbulent viscosity μ_t is determined as:

$$\mu_t=\bar{\rho}C_\mu\frac{k^2}{\varepsilon} \tag{17}$$

where C_μ is a constant.

2.2.2 Geometric model

The geometric models were generated by modeling the interior flow region of the vortex tube working fluid using a conventional CAD software. Some simplifications of the vortex tube geometry were performed to allow the generation of a simpler and more robust computational mesh, without implying great inaccuracies of the CFD model, as done by researchers such as Manimaran (2017) and Rafiee and Sadeghiazad (2017):

a) Simplification of the vortex chamber, only modelling the inlet nozzles region;
b) Simplification of the hot end using an annular region.

As example, the geometric model used for vortex tube with four inlet nozzles is presented in Figure 3.

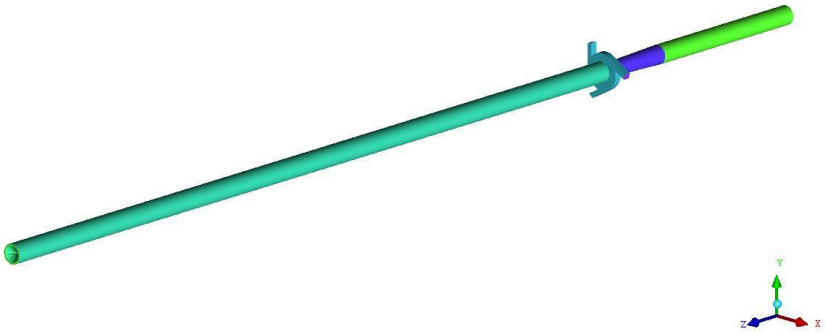

Figure 3. Geometric model for the vortex tube.

2.2.3 Boundary conditions

The boundary conditions applied in the simulations are shown below:

a) The nozzles surfaces were set as the mass flow measured in the experiments;
b) The surface at the end of the extension tube installed at the cold end had its pressure value determined by experimental data;
c) The hot end had its pressure adjusted to reach the air mass fraction measured in the experimental study;
d) Other surfaces were set as adiabatic.

2.2.4 CFD solver

In order to solve the governing equations using CFD techniques, FLUENT® was employed. A Secord-Order Upwind (SOU) was used to quantify convective terms in the transport equations. The Simple algorithm (*Semi-Implicit Method for Pressure-Linked Equations*) was utilized as it is widely used to solve Navier-Stokes equations by coupling the pressure and velocity fields. Because its robustness and versatility the Segregated Pressure-Bases Solver of FLUENT® was adopted.

2.2.5 Computational mesh

The computational meshes employed in the simulations were constructed using ICEM® mesh generator software, which allows creation of hexahedral elements, instead of tetrahedral elements (mesh type commonly used because of its ease of creation), reducing the number of elements of the mesh and computational costs involved in the simulation. In order to do so, mesh building strategy called “blocking” was used, which divides the geometry of the problem into several simple blocks, allowing the generation of hexahedral elements.

Meshes with 500,000 to 2,500,000 elements were tested under the same boundary conditions. A convergence study was performed and it showed that a mesh with 1,800,000 cells ensures CFD results significantly unaltered by further increasing the grid. Also, y+ mean value on the main tube surface remained under 1 with the use of that mesh. This indicates a good discretization of near-wall regions.

3. RESULTS

Some results obtained from the vortex tube simulation and experimental tests are shown below.

3.1 Vortex tube simulation at 2 bar

The vortex tube with 3 inlets at 2 bar was simulated using CFD to evaluate its performance at different cold air fractions. Results from the vortex tube simulations at different cold air fractions (α) compared to experimental data are shown in Fig. 4 and 5.

Fig. 4 represents ΔT_c generated by the vortex tube at its cold end and Fig. 5 shows ΔT_h obtained at the hot end. In these graphics it is observed that the simulated ΔT_c results follow quite well the experimental data with maximum error

of 10%. However, the CFD model predicts lower ΔT_h values at the hot end, with maximum error of 32%. Simulation results showed an accurate prediction of maximum ΔT_c at α of about 50%.

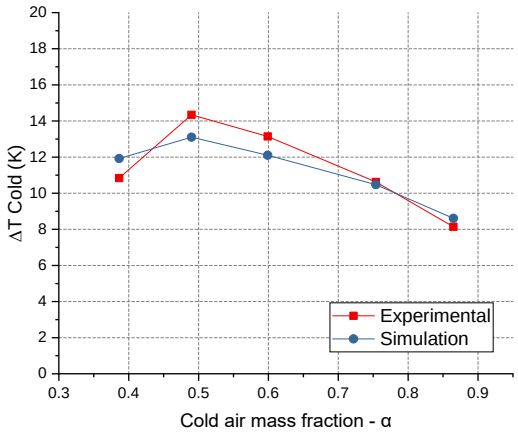

Figure 4. ΔT_c obtained from vortex tube at 2 bar.

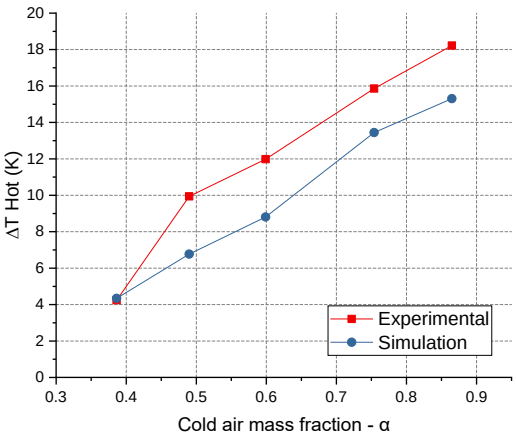

Figure 5. ΔT_h obtained from vortex tube at 2 bar.

Figure 6 to 10 present total temperature, static temperature, velocity and Mach fields in the vortex tube for the cold air fraction of 50%, point of maximum ΔT_c. All these graphics were scaled in Z to allow a better visualization.

The hot end region has the highest total temperature in the whole domain, 318 K, 18 K above the inlet air temperature. This total temperature maximum value is similar to the static temperature at the same region. It happens as a result of a low Mach number, leading total temperature value to its static value.

At the vortex tube cold end and at its downstream there is a cold core at low velocity with total temperature of about 295 K and a hotter outer region at higher Mach number. In that region, the total temperature values are higher than that from static temperature field since its Mach number is near 1, where there is occurrence of subsonic flow.

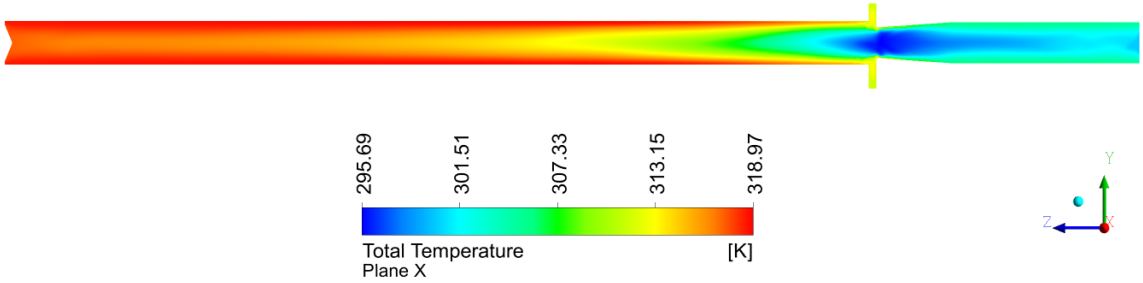

Figure 6. Total temperature in the vortex tube with 3 inlets at 2 bar and α of 50 %.

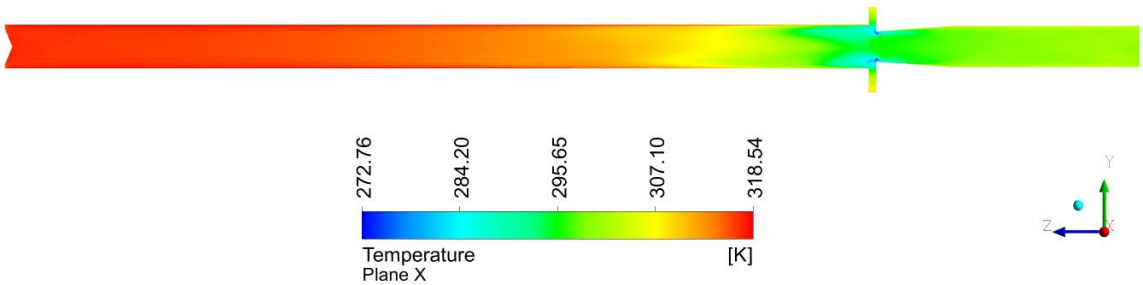

Figure 7. Static temperature in the vortex tube with 3 inlets at 2 bar and α of 50 %.

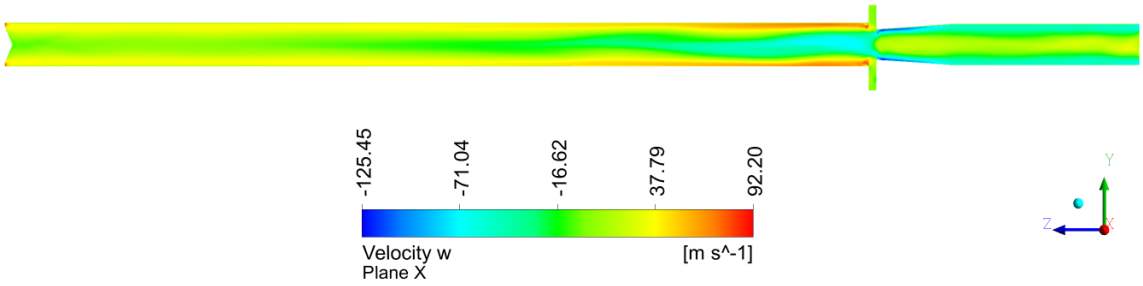

Figure 8. Velocity Z in the vortex tube with 3 inlets at 2 bar and α of 50 %.

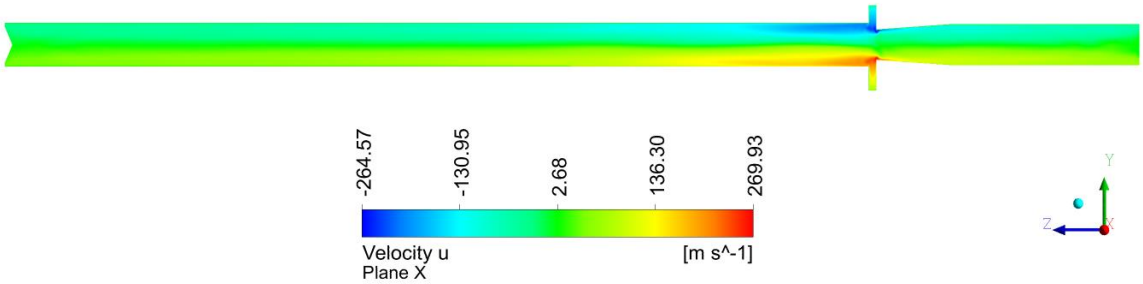

Figure 9. Velocity X in the vortex tube with 3 inlets at 2 bar and α of 50 %.

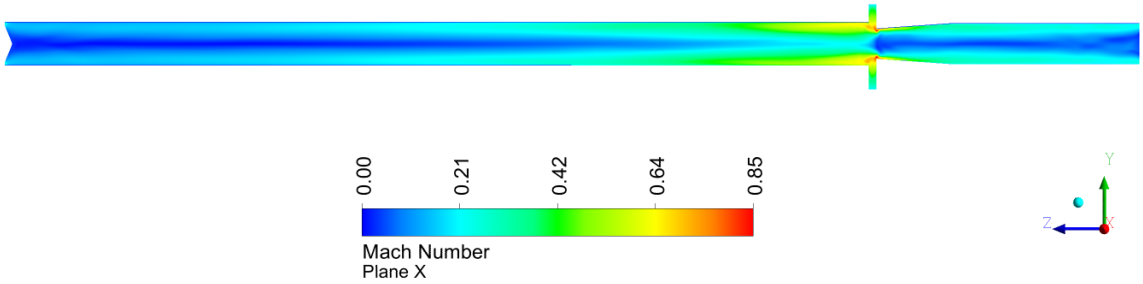

Figure 10. Mach number in the vortex tube with 3 inlets at 2 bar and α of 50 %.

3.2 Vortex tube simulation at 3 bar

CFD simulations from vortex tube with 3 inlets at 3 bar were conducted successfully. Simulations of vortex tube at 3 bar with α ranging from nearly 0.30 to 0.95 are shown in Fig. 11 and 12.

Results showed a good accordance between experimental and simulation data. Furthermore, simulation predicted well the cold air fraction point for the highest ΔT_c. However, simulation predicted thermal separation in a higher magnitude than experimental tests.

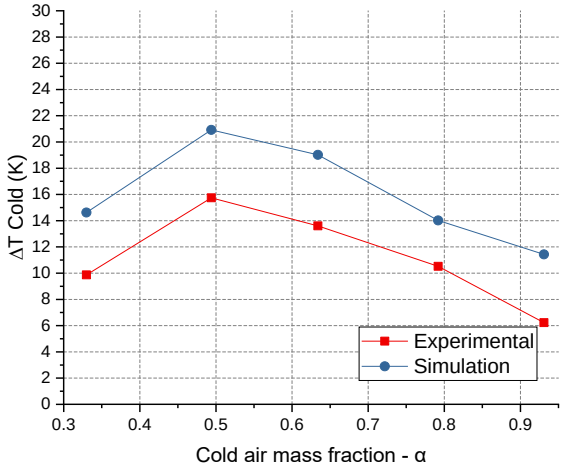

Figure 11. ΔT_c obtained from vortex tube at 3 bar.

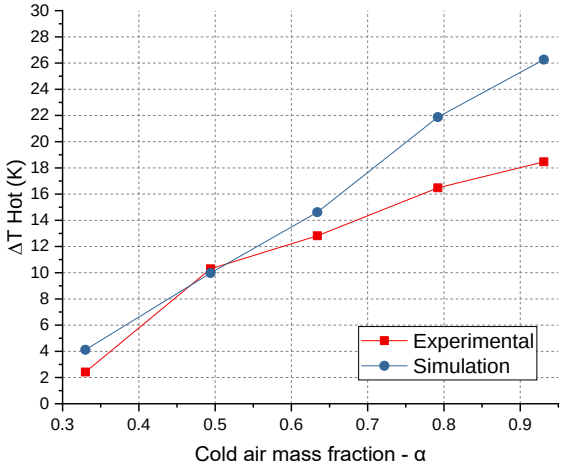

Figure 12. ΔT_h obtained from vortex tube at 3 bar.

Figures 13 to 17 show total temperature, static temperature, velocity and Mach fields in the vortex tube for α at 50%. Total temperature field in Figure 13 presents higher and lower temperatures at hot end and cold end, respectively, than vortex tube simulation at 2 bar in Figure 6 as a result of pressure increase. The same happens for static temperature field.

Velocity fields for 3 bar simulations presents higher values than that found for 2 bar. Furthermore, Mach number field reaches in some regions a sonic flow with Mach above 1.

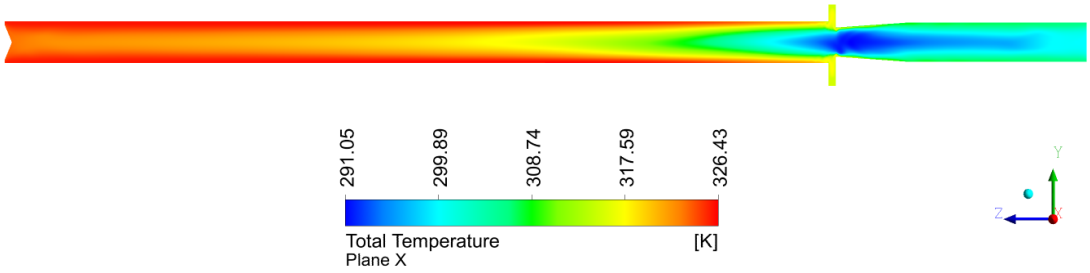

Figure 13. Total temperature in the vortex tube with 3 inlets at 3 bar and α of 50 %.

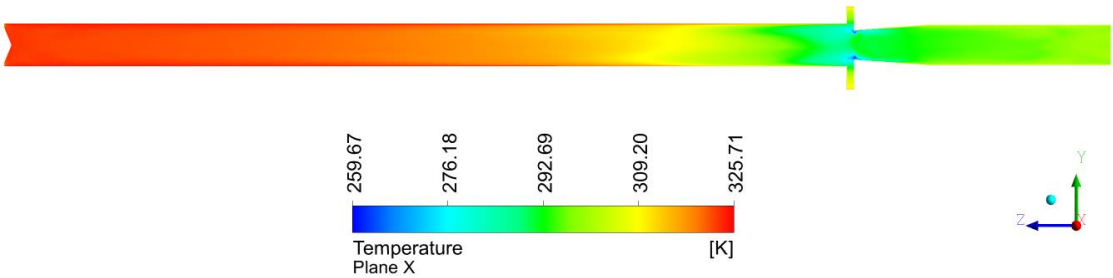

Figure 14. Static temperature in the vortex tube with 3 inlets at 3 bar and α of 50 %.

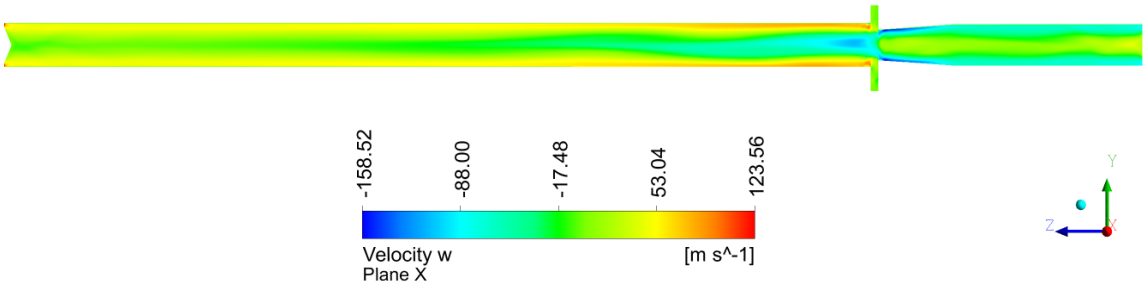

Figure 15. Velocity Z in the vortex tube with 3 inlets at 3 bar and α of 50 %.

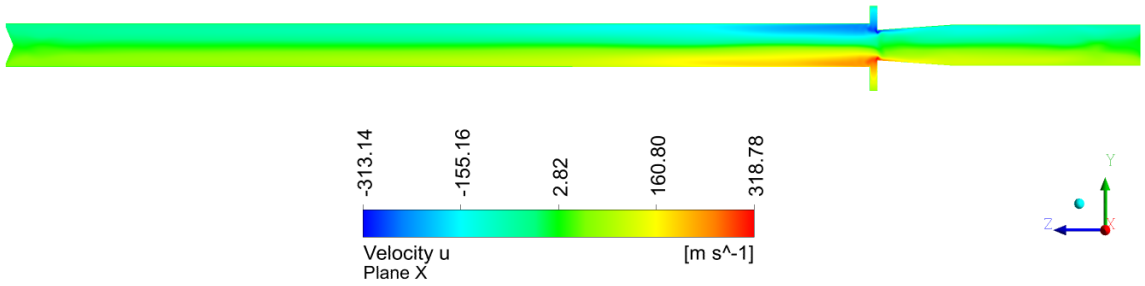

Figure 16. Velocity X in the vortex tube with 3 inlets at 3 bar and α of 50 %.

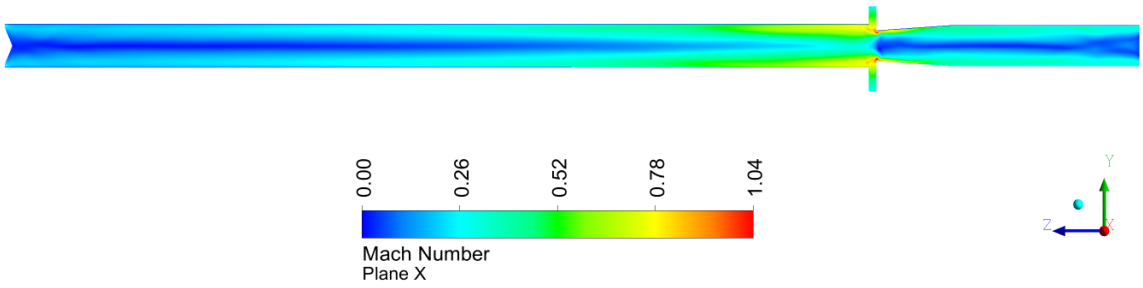

Figure 17. Mach number in the vortex tube with 3 inlets at 3 bar and α of 50 %.

3.3 Vortex tube simulation at 4 bar

As done by the 2 bar and 3 bar simulations, the same procedure was applied for vortex tube with an inlet pressure of 4 bar. Figure 18 and 19 shows, respectively, ΔT_c and ΔT_h found by simulations and experimental tests varying cold air fraction.

Once more, the thermal separation magnitude was predicted by simulations in a higher magnitude than expected. Even so, ΔT_c from simulations has a good accordance with experimental data with regard to shape nevertheless its error. Again, the point of maximum ΔT_c from simulations and experiments is coincident. However, ΔT_h obtained by simulations is quite different than that found by experimental data.

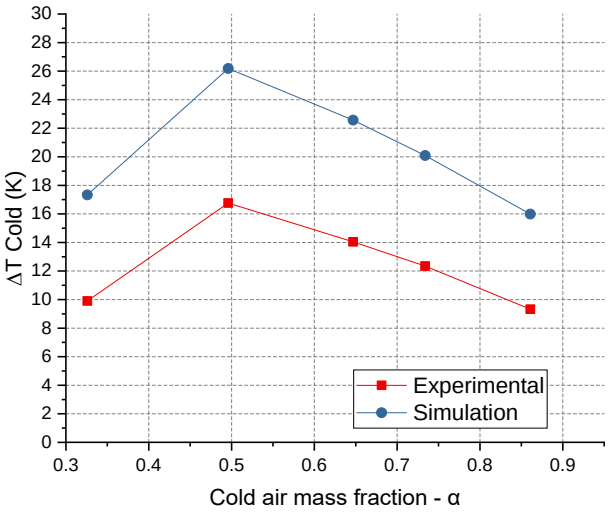

Figure 18. ΔT_c obtained from vortex tube at 4 bar.

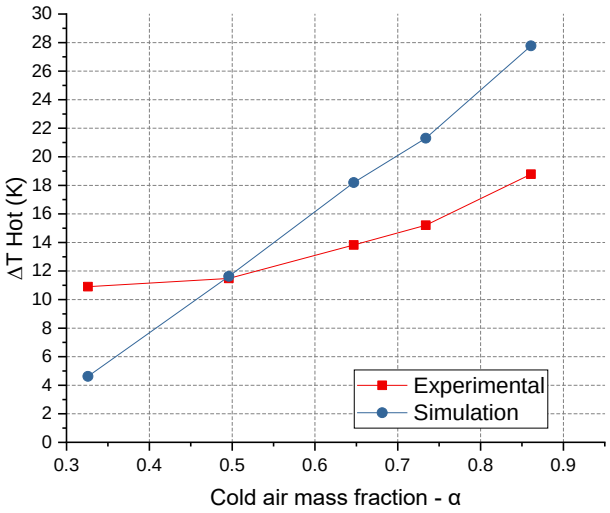

Figure 19. ΔT_h obtained from vortex tube at 4 bar.

Figures 20 to 24 show total temperature, static temperature, velocity and Mach fields in the vortex tube for α at 50%, the point at maximum ΔT_c found by simulations and experiments.

For all simulation at α of 50% so far, Figure 20 shows the minimum total temperature found at cold end core, 289.65 K, and the highest at hot end, 322.56 K.

Velocity X and Z and Mach number fields have its minimum and maximum values increased if compared with 2 and 3 bar simulations.

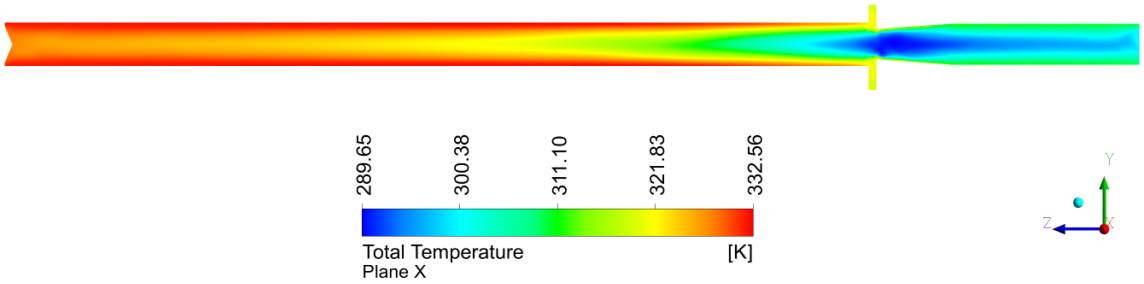

Figure 20. Total temperature in the vortex tube with 3 inlets at 4 bar and α of 50 %.

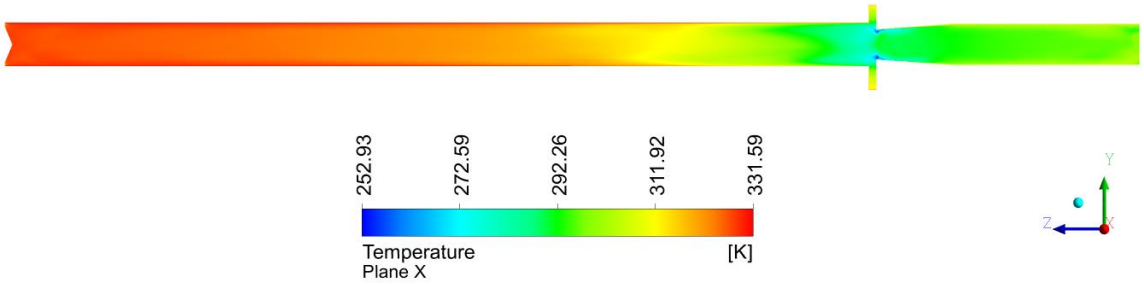

Figure 21. Static temperature in the vortex tube with 3 inlets at 4 bar and α of 50 %.

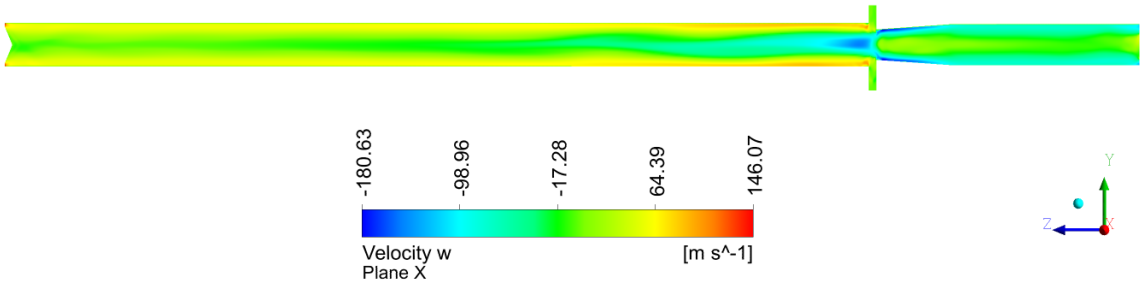

Figure 22. Velocity Z in the vortex tube with 3 inlets at 4 bar and α of 50 %.

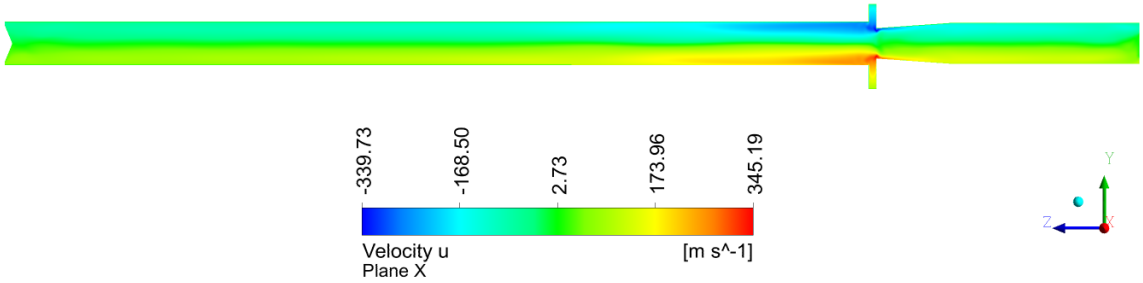

Figure 23. Velocity X in the vortex tube with 3 inlets at 4 bar and α of 50 %.

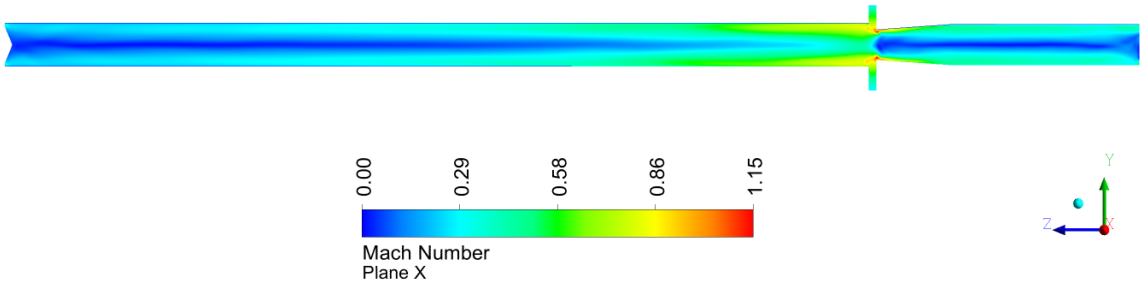

Figure 24. Mach number in the vortex tube with 3 inlets at 4 bar and α of 50 %.

4. CONCLUSIONS

Results obtained from simulations of vortex tube with 3 inlets nozzles showed the occurrence of separation temperature effect and a good accordance with experimental data at 2 bar. For 3 and 4 bar inlet pressures, CFD simulations predicted thermal separation in a higher magnitude than experimental data.

It is suggested to use other turbulence models to investigate the overestimation of thermal separation effect in the vortex tube with 3 inlets.

5. ACKNOWLEDGEMENTS

The authors would like to thank the “Internal Combustion Engine Laboratory” (LMCI) from the Federal University of Ceará for their support.

6. REFERENCES

Behera, U. et al., 2005. "CFD analysis and experimental investigations towards optimizing the parameters of Ranque-Hilsch vortex tube". *International Journal of Heat and Mass Transfer*, v. 48, n. 10, p. 1961–1973.

Behera, U. et al., 2008. "Numerical investigations on flow behaviour and energy separation in Ranque-Hilsch vortex tube". *International Journal of Heat and Mass Transfer*, v. 51, n. 25–26, p. 6077–6089.

Dutta, T., Sinhamahapatra, K. P. and Bandyopadhyay, S. S., 2001. "Numerical investigation of gas species and energy separation in the Ranque-Hilsch vortex tube using real gas model". *International Journal of Refrigeration*, v. 34, n. 8, p. 2118–2128.

Hilsch, R., 1947. "The Use of the Expansion of Gases in a Centrifugal Field as Cooling Process". *Review of Scientific Instruments*, v. 18, n. 2, p. 108–113.

Kandil, H. A. and Abdelghany, S. T., 2015. "Computational investigation of different effects on the performance of the Ranque-Hilsch vortex tube". *Energy*, v. 84, p. 207–218.

Manimaran, R., 2017. "Computational analysis of flow features and energy separation in a counter-flow vortex tube based on number of inlets". *Energy*, v. 123, p. 564–578.

Ouadha, A., Baghdad, M. and Addad, Y., 2013. "Effects of variable thermophysical properties on flow and energy separation in a vortex tube". *International Journal of Refrigeration*, v. 36, n. 8, p. 2426–2437.

Pouraria, H. and Zangooee, M. R., 2012. "Numerical investigation of vortex tube refrigerator with a divergent hot tube". *Energy Procedia*, v. 14, n. 2011, p. 1554–1559.

Rafiee, S. E. and Rahimi, M., 2013. "Experimental study and three-dimensional (3D) computational fluid dynamics (CFD) analysis on the effect of the convergence ratio, pressure inlet and number of nozzle intake on vortex tube performance-validation and CFD optimization". *Energy*, v. 63, p. 195–204.

Rafiee, S. E. and Sadeghiazad, M. M., 2014. "Three-dimensional and experimental investigation on the effect of cone length of throttle valve on thermal performance of a vortex tube using k-ε turbulence model". *Applied Thermal Engineering*, v. 66, n. 1–2, p. 65–74.

Rafiee, S. E. and Sadeghiazad, M. M, 2017. "Experimental and 3D CFD investigation on heat transfer and energy separation inside a counter flow vortex tube using different shapes of hot control valves". *Applied Thermal Engineering*, v. 110, p. 648–664.

Ranque, G. J., 1933. "Experiments on expansion in a vortex tube simultaneous of hot air and cold air". *J. Phys. Radium*, p. 112–114.

Skye, H. M., Nellis, G. F. and Klein, S. A., 2006. "Comparison of CFD analysis to empirical data in a commercial vortex tube". *International Journal of Refrigeration*, v. 29, n. 1, p. 71–80.

Secchiaroli, A. et al., 2009. "Numerical simulation of turbulent flow in a Ranque–Hilsch vortex tube". *International Journal of Heat and Mass Transfer*, v. 52, n. 23, p. 5496–5511.

Thakare, H. R. and Parekh, A. D., 2015. "Computational analysis of energy separation in counter-flow vortex tube". *Energy*, v. 85, p. 62–77.

Shamsoddini, R. and Nezhad, A. H., 2010. "Numerical analysis of the effects of nozzles number on the flow and power of cooling of a vortex tube". *International Journal of Refrigeration*, v. 33, n. 4, p. 774–782.

7. RESPONSIBILITY NOTICE

The authors are the only responsible for the printed material included in this paper.